Improved Performance of Multilayer Neutron Monochromator by Addition of Hydrogen in Titanium Layer

The current neutron guides and super mirrors are made of alternatively repeating $Ni-C$ and Ti Multilayer(ML) coating. The most important factors required to obtain the high-performance reflectivity from neutron guide or super mirror coating are to select proper materials with the large scattering length density contrast, to regulate the bilayer thickness, and to maintain each layer as smooth and flat as possible. One of the methods to improve the neutron reflectivity is enhancing the contrast between two deposition components. The scattering length densities of Ni, Ti, and H are $9.41 \times 10^{-6}\text{Å}^{-2}$, $-1.95 \times 10^{-6}\text{Å}^{-2}$, and $-2.01 \times 10^{-6}\text{Å}^{-2}$ respectively. Therefore, the improvement can be obtained by the addition of hydrogen atoms into Ti layers, to form the titanium hydride (TiH_2), the scattering length density of which is ideally $-5.14 \times 10^{-6}\text{Å}^{-2}$. Two parallel sets of multi-layer(ML) films, with- and without-hydrogen, were prepared by a magnetron sputtering technique. The number of bilayers(BLs) in each series was varying from 1 to 40, with a typical bilayer spacing of 84Å. All the samples were measured at POSY II, Intense Pulsed Neutron Source, Argonne National Laboratory. The neutron reflectivity comparison between two parallel sets demonstrates that the first order Bragg's peak intensities of all with-hydrogen samples were significantly elevated by 64 % on average and the maximum intensity was observed up to 56.1 % at the $k_z = 0.0383$ Å^{-1}. The peak intensities of both Ni/Ti and Ni/TiH_2 systems were lower than the theoretical as the more layers were deposited. The roughness of the films mainly causes the drop of the reflectivity performance. The blurriness of the interfaces between Ni and Ti layers was observed by Auger Electron Spectroscopy(AES) and the existence of hydrogen in Ti layers shapened the interfaces. The formation of TiH_2 in the with-hydrogen samples was confirmed consistently with the data fit analysis onto the neutron reflectivity. The purpose of this work will focus on the neutron reflectivity response, including the data-fits, the correlation between the neutron reflectivity performance and the

hydrogen incorporation, and the AES results.

Table of Contents

List of Tables . . . . . **iv**

List of Figures . . . . . **v**

0.1 Introduction 1

0.2 Experiments 7

0.2.1 Sample preparation 7

0.2.2 Auger electron spectroscopy depth profiling (AESDP) 9

0.2.3 Neutron reflection (NR) 13

0.3 Analysis and Discussion 16

0.3.1 Neutron scattering length densities from data-fit 16

0.3.2 Enhanced contrast between neutron scattering length densities 20

0.3.3 Improved interfacial roughness 22

0.3.4 Interfacial roughness analysis 23

0.4 Conclusion 28

Bibliography **30**

List of Tables

1 Neutron properties of materials 9
2 Results from neutron reflectivity measuremnts of all samples 10

List of Figures

1 Reflectivity of a single layer on the substrate and the critical angle of the total external reflection . . . 2
2 A scheme of depth profile in a multilayer monochromator . . . 3
3 Reflection from a multilayer monochromator with a single bilayer spacing d and scattering length density contrast $\Delta\rho b$ . . . 4
4 Continuously varying d-spacing in the ML extends the critical edge : a) a scheme of supermirror and b) actual response of the supermirror film of NiC-Ti by Hino et al.(2004) . . . 7
5 Slow AESDP Results of MH20 and MH40 sputtered at 750eV . . . 12
6 Scheme of *POSYII* . . . 13
7 Detailed scheme of ^{58}Ni filters installed at *POSYII* . . . 14
8 The time-dependent spectrum of the neutron beam of POSYII . . . 15
9 Neutron reflectivity data-fit of 2BL and 4BL . . . 17
10 Neutron reflectivity data-fit of 6BL and 10BL . . . 18
11 Neutron reflectivity data-fit of 20BL and 40BL . . . 19
12 Reflectivity analysis . . . 21
13 Debye-Waller factor analysis . . . 24
14 Interface comparison from the bottom layer to the top Layer . . . 25
15 f_o/f parameters of 20 BLs . . . 27

0.1 Introduction

Neutron optics device generally plays a role to define the neutron beam conditions such as direction, divergence, energy, etc. The defining method should be efficiently employed due to the low primary neutron flux[1]. Among the basic neutron optics devices, a collimator is used to define the direction and divergence of a neutron beam. The simpliest collimators consist of a pinhole in an absorbing plate or two absorbing slits and are placed at both ends of the neutron beam path. A parasitical scattering from the edge of the collimator may occur to interfere the primary neutron beam so that very thin sheets of a highly absorbing material should be used. In order to select a well-defined energy band from a white neutron beam, Bragg reflection from a crystal[1] is most widely employed in the monochromation technique. Reflection from a perfect crystal can easily define a neutron beam with a single wavelength. A reasonably high reflected intensity is required in the most of neutron applications. Thus, a trade-off between the reflected intensity and the energy band pass should be made to obtain a high reflected intensity. A mosaic crystal is commonly preferred to a perfect crystal, even though a mosaic crystal increases beam divergence and leads to beam broadening. Due to a demand on the higher reflectivities, neutron monochromators are usually set to be used in reflection geometry rather than transmission geometry. Based on the principle of mirror reflection, neutron guides are used to deliver neutrons to a sample stage where the neutron instrument is installed. Neutron guide is usually operated in vacuum to avoid losses in neutron beam intensity due to scattering and absorption of neutrons in air. Neutrons are reflected a number of times while the neutron guide transmits a neutron beam. Thus, it is important to obtain and maintain the high reflectivity during transmitting neutrons away from the source.

For a single thick layer on the substrate, the reflectivity of the film is determined by the following Eq.(1)[2], shown in the Fig. 1.

[1] *Bragg*'s Law $n\lambda = 2d\,\sin\theta$

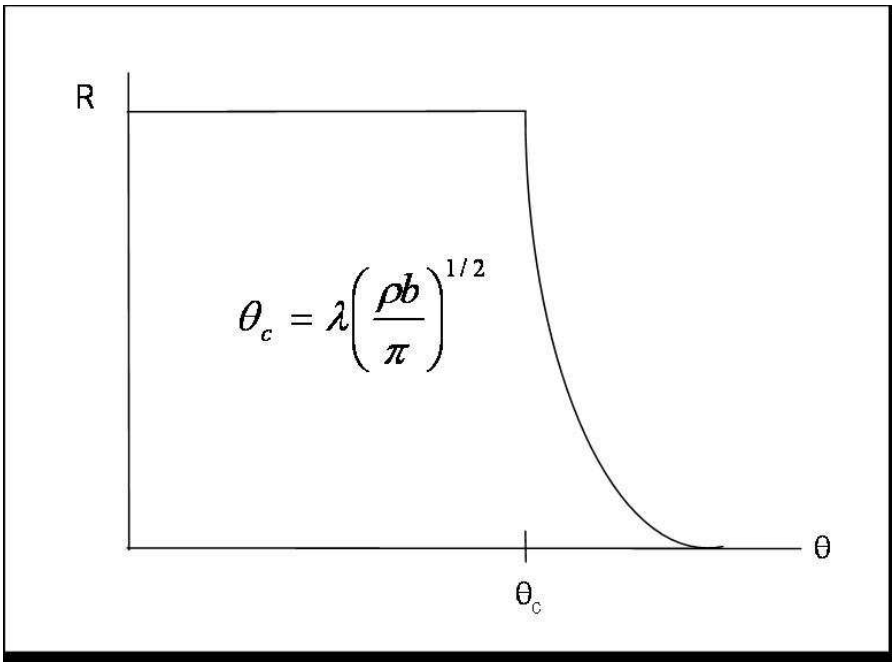

Figure 1: Reflectivity of a single layer on the substrate and the critical angle of the total external reflection

$$R = \left| \frac{\left[(n^2 - \cos^2\theta)^{1/2} - \sin\theta \right]}{\left[(n^2 - \cos^2\theta)^{1/2} + \sin\theta \right]} \right|^2 \tag{1}$$

where λ is a wavelength of neutrons and $\Delta\rho b$ is the SLD contrast between the components. The neutron scattering length density b denotes the media effective potential V, given by *Lekner*[3]

$$V = \left(\frac{\hbar^2}{2m}\right) 4\pi\rho b \tag{2}$$

and the refractive index is expressed as

$$n^2 = 1 - \frac{\lambda^2 \rho b}{\pi} \tag{3}$$

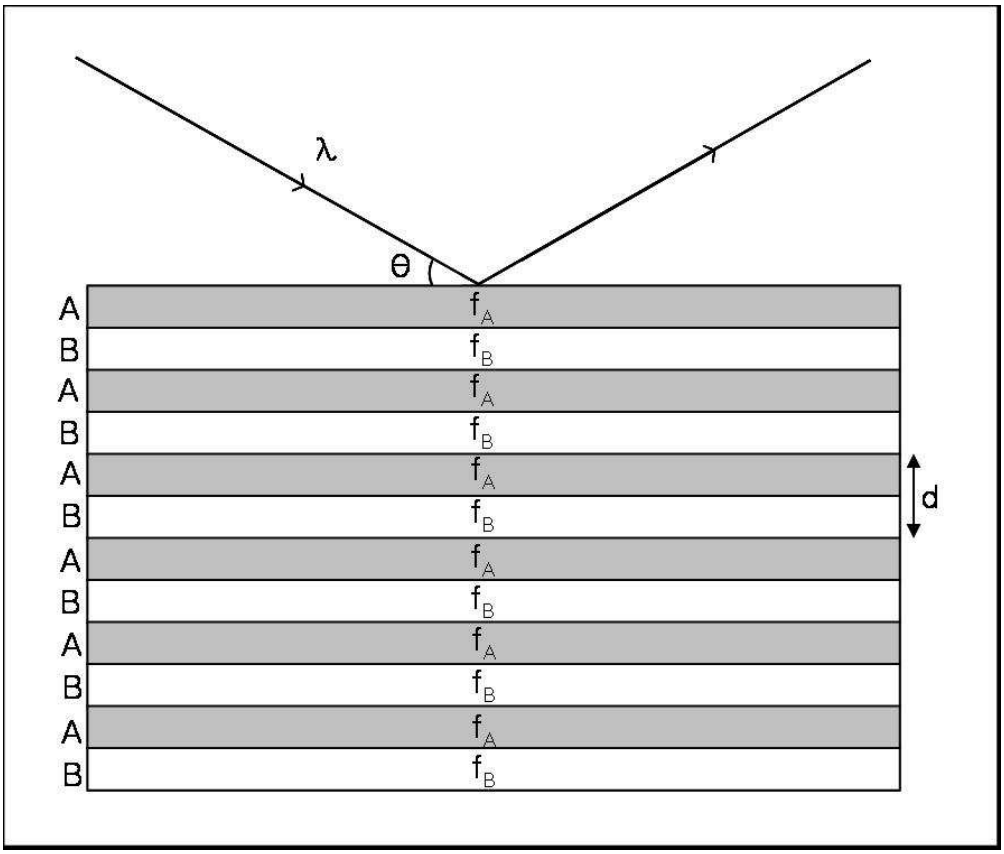

Figure 2: A scheme of depth profile in a multilayer monochromator

The critical angle for total external reflection is defined as[4]

$$\theta_c = \lambda \left(\frac{\Delta \rho b}{\pi} \right)^{\frac{1}{2}} \tag{4}$$

A multilayer(ML) structure alternatively deposited with two materials of different neutron scattering length densities(SLD) can also define a monochromatic beam[5]. The ML monochromator ideally has a single bilayer spacing, a large SLD contrast, low absorption, incoherent and inelastic cross sections as shown in Fig. 2.

Fig. 3 shows that Bragg's reflection from the ML is correspondent to the bilayer spacing periodically repeated. With careful selection of proper materials comprising alternatively stratified ML architecture, the reflectivity of close to 100% can be obtained. A ML system based on Ni/Ti system is typically employed to fabricate a neutron monochromator due to

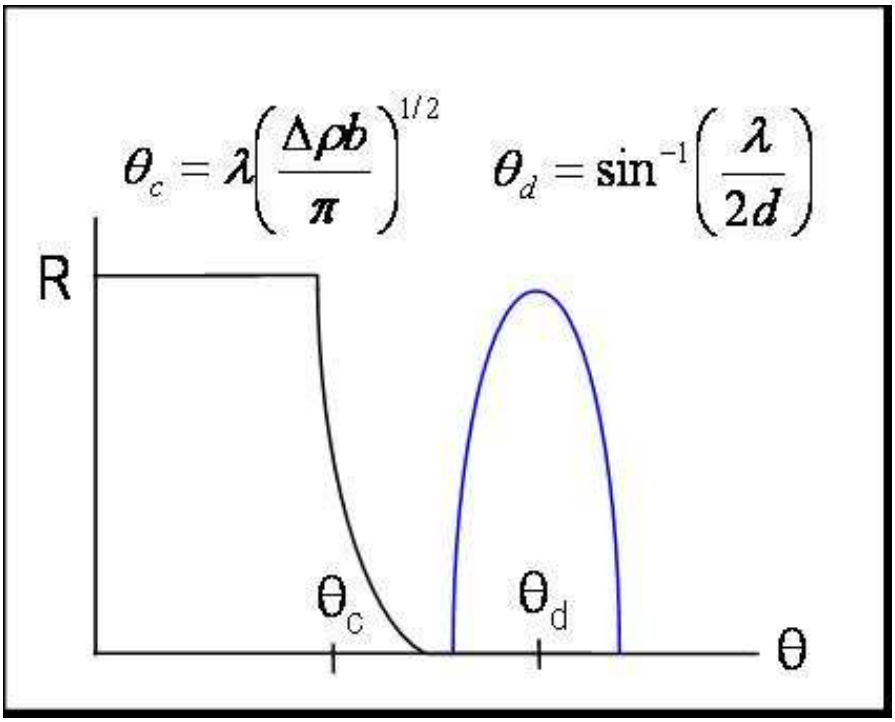

Figure 3: Reflection from a multilayer monochromator with a single bilayer spacing d and scattering length density contrast $\Delta\rho b$

a large SLD contrast[5, 6, 7, 8, 4, 3, 2, 9, 10, 11, 12].

The reflectivity expression for the ML was evaluated from a *Fresnel* zone construction by *Saxena and Schoenborn*[9].

$$R = |A|^2 \tag{5}$$

where

$$A = \frac{4\pi}{q_z}\int_0^D f(z)\exp(iq_z z)\,dz \tag{6}$$

and $D \equiv D_z$ is the thickness of the ML. From Fig. 2, $f(z)$ for the ideal ML is a periodic function with period d.

$$f(z) = f(z+d) \tag{7}$$

Especially, in the case of bilayer structure(BL),

$$f(z) = \begin{cases} f_A = \rho_A b_A\,, & 0 < z < sd \quad \text{in the A layers} \\ f_B = \rho_B b_B\,, & sd < z < d \quad \text{in the B layers} \end{cases} \tag{8}$$

s is the fractional thickness of the A layer. Then the unit BL structural factor from the following definition ,

$$F(q_z) = \frac{1}{d}\int_0^d f(z)\exp(iq_z z)\,dz \tag{9}$$

can be evaluated to the following expression for this BL model.

$$F_m = \begin{cases} f_A s + f_B(1-s)\,, & m = 0 \\ (f_A - f_B)\left[\exp(2ms\pi i) - 1\right]/2m\pi i\,, & m \neq 0 \end{cases} \tag{10}$$

If the fractional thickness of the A layer, s, is $\frac{1}{2}$ and the interfaces are ideally sharp[6], then

$$|F_m|^2 = \begin{cases} \left[\frac{(f_A+f_B)}{2}\right]^2 & m = 0, \\ 0 & m = \pm 2,\ \pm 4,\ \cdots, \\ \left[\frac{(f_A-f_B)}{m\pi}\right]^2 & m = \pm 1,\ \pm 3,\ \cdots \end{cases} \tag{11}$$

Thus, the even-order reflections are extinct and the odd-order reflections are expressed as[5, 6].

$$R_m(max) = \left[\frac{2Nd^2(f_A - f_B)}{\pi m^2}\right] \tag{12}$$

In the case of a sinusoidally varying the scattering length density in the ML[6],

$$f(z) = \frac{1}{2}\left[(f_A + f_B) + (f_A - f_B)\sin\left(\frac{2\pi z}{d}\right)\right] \tag{13}$$

Hence,

$$|F_m|^2 = \begin{cases} \left[\frac{(f_A+f_B)^2}{2}\right]^2 & , \ m = 0, \\ \left[\frac{(f_A-f_B)^2}{4}\right]^2 & , \ m = \pm 1, \\ 0 & , \ m = \pm 2, \ \pm 3, \ \cdots \end{cases} \tag{14}$$

Sinusoidally blurred interfaces in the ML leads to extinguish all the higher-order reflections except the first-order and the intensity of the first-order reflection is reduced by a factor of $\left(\frac{\pi}{4}\right)^2 \simeq 0.617$, compared to the ideal ML structure with the fractional thickness, $s = \frac{1}{2}$[5, 6, 8].

The above results about neutron reflectivity are all evaluated with the kinematic theory of neutron scattering, which considers only single scattering in the media. These results require that $Nd \ll \Delta \equiv m\pi/2d\,|F_m|$ for validity of $R_m\,(max) \ll 1$. Supposed multiple scattering and the extinction effects are considered with the dynamic theory of neutron diffraction, the $m^{\,th}$-order reflections are evaluated for the same multilayer structure with Fig. 2 as[6]

$$R_m = \frac{\sin^2\left[y\,(x^2-1)^{\frac{1}{2}}\right]}{x^2 - 1 + \sin^2\left[y\,(x^2-1)^{\frac{1}{2}}\right]} \tag{15}$$

where

$$\begin{aligned} x &\equiv \frac{\pi m\left(q_z - \frac{4\pi}{\lambda_m}\sin\theta\right)}{4\pi d|F_m|} \\ y &\equiv \frac{2Nd^2|F_m|}{m\pi} \end{aligned} \tag{16}$$

Therefore, the m^{th}-order diffraction peak reflectivity is given by

$$R_m\,(max) = \tanh^2 y = \tanh^2\left(\frac{2Nd^2\,|F_m|}{m}\right) \tag{17}$$

The specific ML film with a sinusoidal profile can produce a high intense reflectivity only at the 1st order diffraction angle so that it can be used for a high performance monochromator[6, 7, 13, 8]. In this case, the critical angle of a ML architecture can be extended to $\theta = m\,\theta_c$ (m = integer) by continuously varying the bilayer spacing, often called

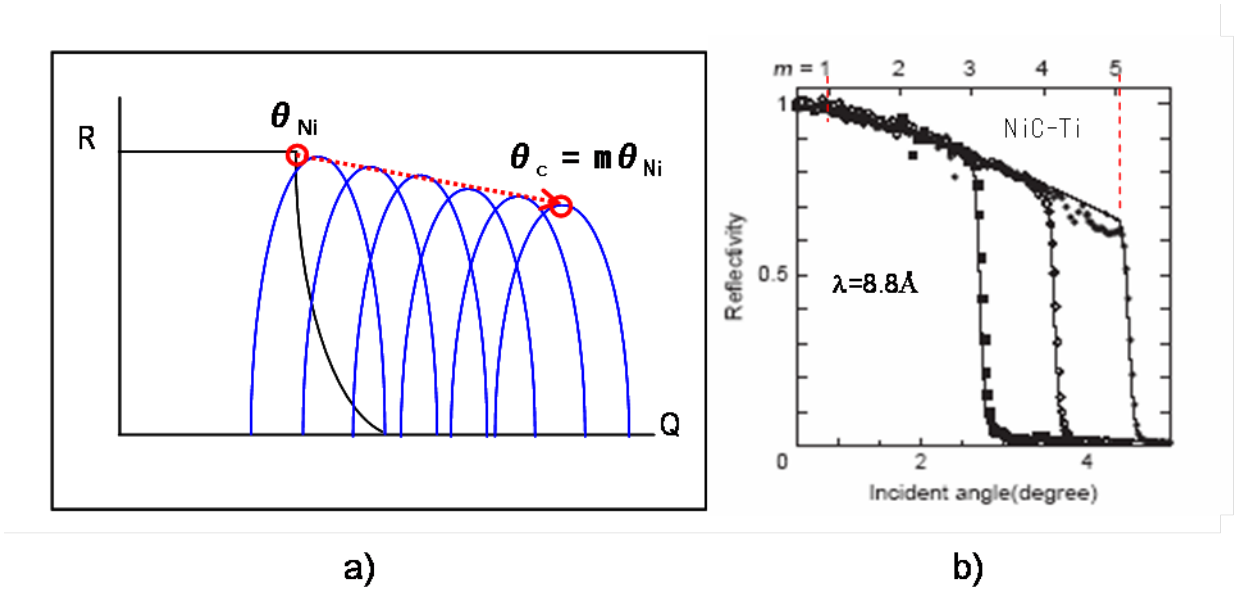

Figure 4: Continuously varying d-spacing in the ML extends the critical edge : a) a scheme of supermirror and b) actual response of the supermirror film of NiC-Ti by Hino et al.(2004)

a *supermirror* shown in Fig. 4. At the end of the guide, coated with a supermirror film structure, the flux can be gained at the order of m^2. Thus, the flexibility to change the SLD profile and the bilayer spacing can greatly benefit to fabricate the neutron optics devices using the principle of mirror reflection.

0.2 Experiments

0.2.1 Sample preparation

The most important parameters for selecting appropriate materials are the large SLD contrast, $\triangle\rho b$, between two selected materials and the solubility of hydrogen in the material with negative b_c. The neutron properties of the most common materials in neutron optics devices are tabulated[2]. Shown in the Table1, Ti is one of few materials that have a negative neutron scattering length, b_c, and a fairly high hydrogen capacity, $H/M = 1.97$ $(3.9\ wt.\%)$. Ni would be the best selection for this purpose since Ni naturally has the highest b_c and even the co-

[2] b_c refers to the NIST web site : http://www.ncnr.nist.gov/resources/sldcalc.html

herent cross section, $\sigma_{coh} = 4\pi b_c^2$, is higher than the coherent cross section of Be. The main approach here is to add H atoms into Ti layers and enlarge the contrast $\triangle\rho b$ between Ni and Ti layers. The designed formation of titanium hydride is ultimately TiH_2. TiH_2 formation from pure Ti indispensably experiences a volume expansion as hydrogen atoms immigrate into the interstitial sites of Ti lattices. From the lattice parameters of the stoichiometric body-centered tetragonal TiH_2, the volume per atom is $(3.202)^2 \times 4.279$ Å$^3/2 = 21.936$ Å^3[14] and the volume per atom of pure Ti is 17.668 Å^3[15]. TiH_2 has a cubic lattice with the lattice parameters of 4.42 Å[16] and the volume per atom is 21.588 Å^3. Thus, the volume expansion of $\sim 22.19\%$ occurs during the formation of TiH_2. Two hydrogen atoms in TiH_2 dramatically increases SLD of TiH_2, while the volume expansion relatively reduces the atomic density of TiH_2 compared to Ti. The changes in the atomic density and the scattering length are evaluated as $(\rho b)_{TiH_2} = -5.027 \times 10^{-6}$ Å^{-2}and the reference value from the SLD calculator[3] serviced on the NIST is -5.14×10^{-6} Å^{-2}. Calculating the SLDs of pure Ni, Ti, and Si with the atomic number density ρ and the coherent scattering length density b yields 9.41×10^{-6} Å^{-2}, -1.95×10^{-6} Å^{-2}, and 2.07×10^{-6} Å^{-2}, respectively(Table 1). Thus, the SLD values calculated from the lattice parameters are comparably consistent with the reference SLD values. The contrast would be theoretically enlarged by $\sim 28.1\%$. Starting from the calculated SLD values of Ni, Ti, TiH_2, and Si, the hydrogen effect on the contrast enhancement will be compared and discussed with analyses on the experimental results. Based on the results, the enhanced contrast obviously contributed towards the improved performance of the ML reflectivities.

All the samples were fabricated in *Frederick Seitz Materials Research Laboratory* (FS-MRL), using a DC magnetron sputtering machine(*AJA 2000* co-sputtering system) at the total processing pressure (P_{tot}) 3 mTorr at room temperature. The two parallel sets of samples with and without hydrogen gas were deposited on $(100)Si$ wafer where an oxide layer naturally presents. The DC powers for Ni and Ti target were typically ~ 140 watts

[3]the NIST web site : http://www.ncnr.nist.gov/resources/sldcalc.html

Table 1: Neutron properties of materials

Material	$\rho\,[g/cm^3]$	$b_c\,[fm]$	$\rho b\left[10^{-6}\text{Å}^{-2}\right]$	H/M
H	0.088	-3.741	-1.97	
Be	1.82	7.79	9.47	
C	3.516	6.648	1.17	
O		5.805		
Mg	1.74	5.375	5.72	
Si	2.33	4.151	2.07	
Ti	4.51	-3.37	-1.95	1.97
Mn	7.47	-3.75	-3.05	
Ni	8.91	10.3	9.41	
Cu	8.93	7.718	6.53	
TiH_2	3.90		-5.14	

and $\sim$ 150 watts, respectively. The details of the ML structures obtained from neutron reflectivity experiments are tabulated in the Table 2.

0.2.2 Auger electron spectroscopy depth profiling (AESDP)

Auger electron spectroscopy(AES) is used to analyze surface composition by measuring the energies of Auger electrons[17]. In the process of Auger electron emission with a characteristic energy, three electrons of one-hole initial state and two-hole final state are involved in the transition. Thus, Auger electron emission can allow the identification of materials by measuring the electron energy and Auger transition process can occur at all elements even in low-Z elements except for H and He. Due to the low kinetic energy of Auger electrons, the escape depth of the electrons is limited to a few atomic layer($\sim$ 4nm). Therefore, only the top atomic layers are analyzed. AES can be illustrated by three steps:

1. atoms are ionized by removing a core electrons

2. electrons are emitted through the Auger process

3. analyze the emitted Auger electrons to identify atoms and quantify concentration

Table 2: Results from neutron reflectivity measuremnts of all samples

Sample	Num. of BLs	d [Å]	$\triangle k_z$FWHM [Å^{-1}]	$R_{measured}$	R_{calc}
MH2	2	94	0.0148	0.0162	0.0055
MH4	4	89	0.0083	0.0817	0.0216
MH6	6	78	0.0066	0.0823	0.0326
MH10	10	85	0.0045	0.2080	0.1163
MH20A	20	84	0.0030	0.2840	0.3582
MH20B	20	77	0.0032	0.3480	0.2952
MH40	40	82	0.0023	0.5610	0.7700
M2	2	94	0.0148	0.0102	0.0057
M4	4	87	0.0087	0.0446	0.0223
M6	6	85	0.0065	0.0837	0.0297
M10	10	88	0.0044	0.1710	0.1091
M20A	20	88	0.0027	0.2500	0.3957
M20B	20	75	0.0030	0.1670	0.2712
M40	40	86	0.0032	0.4000	0.7679
M2N	2	91	0.0300	0.0111	0.0045
M4N	4	89	0.0138	0.0317	0.0171
M6N	6	79	0.0111	0.0621	0.0381
M10N	10	78	0.0073	0.1207	0.0943
M20N	20	79	0.0060	0.1821	0.3009
M40N	40	79	0.0067	0.1972	0.7228

M represents for Multilayer and H for Ti Hydride
N means the samples were made of New Ti target
A and B point out two distinct samples in 20 BLs
d-spacing was calculated from NR results,
$d = \frac{2\pi}{Q_B}$, Q_B = 1st order Bragg peak position
$R_{calc} = \tanh^2(2Nd^2\Delta\rho b)$; $\Delta\rho b = (\rho b_{Ni} - \rho b_{Ti})$

Impurities such as oxygen and carbon in Ti layers bring their positive SLD value into the titanium which has naturally a negative value. Thus, those impurities blended into Ti layers lead to reducing the contrast between Ni and Ti layers. The depth profile of the atomic concentration in the samples should be investigated by AESDP and it was performed[4] with Physical Electronics model 660 at *CMM, UIUC*. AES is operated under ultrahigh vacuum and equipped with an in-situ Ar-ion etching gun for depth profiling[18]. The AESDP utilizes an excitation source, *LaB6 Filament Electron Gun*, and the minimum spot size of $\sim$ 100 nm for Auger analysis with 0.5 to 20 keV. The detection system consists of a single pass cylindrical mirror analyzer and a single channel electron multiplier. A differentially pumped Ar ion gun with automatic leak value is used as a sputtering system. Typically, most of AESDP experiments were carried out at 3 keV and the lower voltage scans were additionally performed at 750 eV for closely observing the interface profile between Ni and Ti layers.

The AES analyses on the ML samples were performed to ascertain the impurity existence and quantify the impurity concentration through depth-profiling. In order to scan the interface profiles more precisely, the lower voltage 750 eV of AES was employed, called *slow* AESDP rather than *fast*. Fig. 5 confirm that the impurity levels in the ML samples are restrained well to be ignorable. From the AESDP on the ML samples, the contamination by the impurity is considerable only for the Ti thick film.

AES technique cannot probe H and He atoms due to the principle of the Auger process. Therefore, AESDP does not directly show the hydrogen concentration level in Ti layers. Nevertheless, a flat and reduced constant concentration level of Ti related to the Ni signal through a ML architecture indirectly indicates a uniform composition of TiH_x. The oscillation of the concentration level centered at a constant level presents the interfacial morphology. Thus the sharpness and the intensity of the oscillation peaks may explain the blurriness between the interfacial layers due to the inter diffusion.

[4]All the AES data were obtained by *Nancy Finnegan*, a scientist of CMM, UIUC.

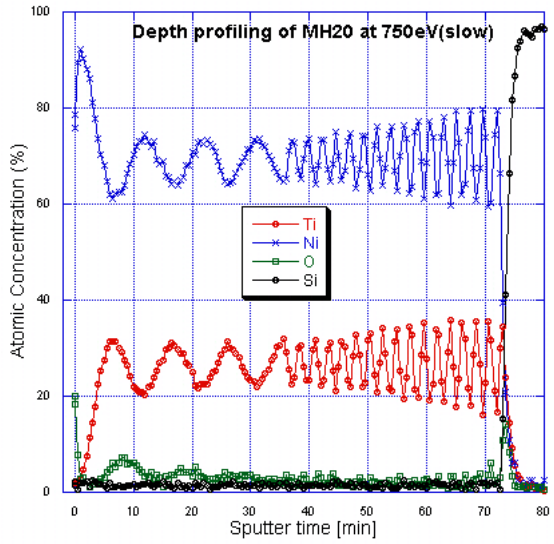

(a) Slow AESDP of MH20

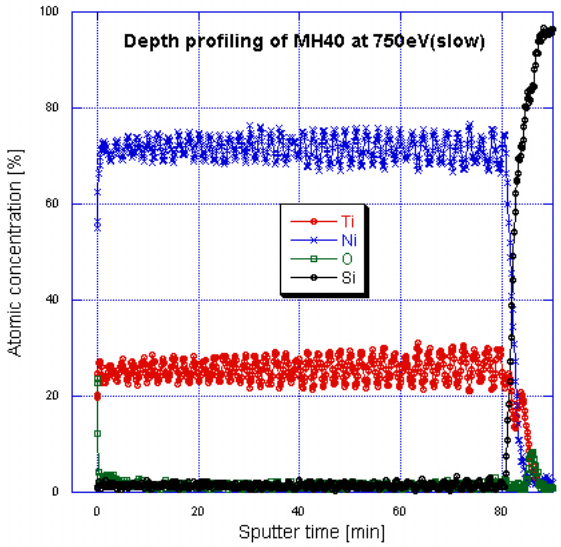

(b) Slow AESDP of MH40

Figure 5: Slow AESDP Results of MH20 and MH40 sputtered at 750eV

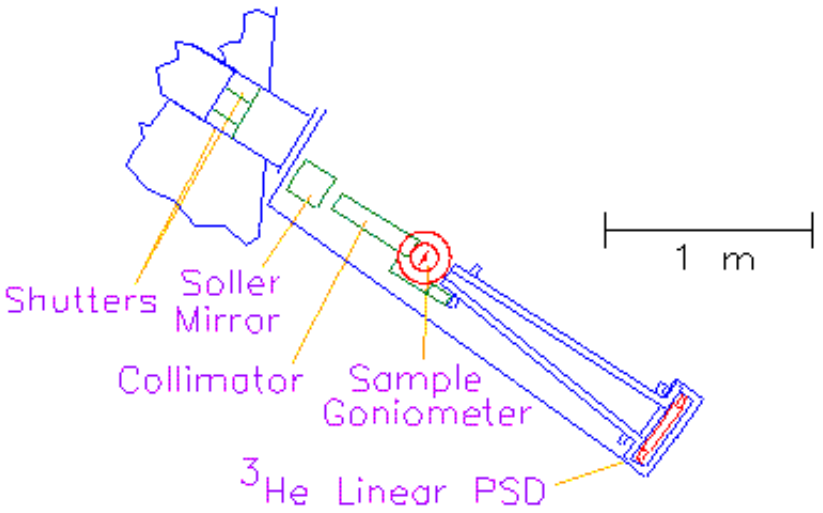

Figure 6: Scheme of *POSYII*
(captured from *POSYII* web site)

0.2.3 Neutron reflection (NR)

A reflectometer is typically designed to study the chemical or magnetic depth profile of the film structures prepared on flat substrates. Neutron reflectivity of all samples was measured with the reflectometer, *POSY II*, at *Intense Pulsed Neutron Source* (IPNS) at *Argonne National Laboratory* (ANL) . *POSYII* is a unpolarized neutron reflectormeter installed at the beam line C2 of IPNS and operated in air.

As shown in the Fig. 6[5], *POSYII* consists of the neutron filter assembly, the sample stage, and the neutron detector[19]. The detector is placed at a distance of $8.9m$ from the source and $\sim 7.9m$ from the moderator. The distance between the sample stage and the detector is $175cm$.

A white neutron beam is generated by a spallation source with a frequency of 30 Hz and

[5]the *POSYII* web site : http://www.posy2.anl.gov/Specifications/specifications.html

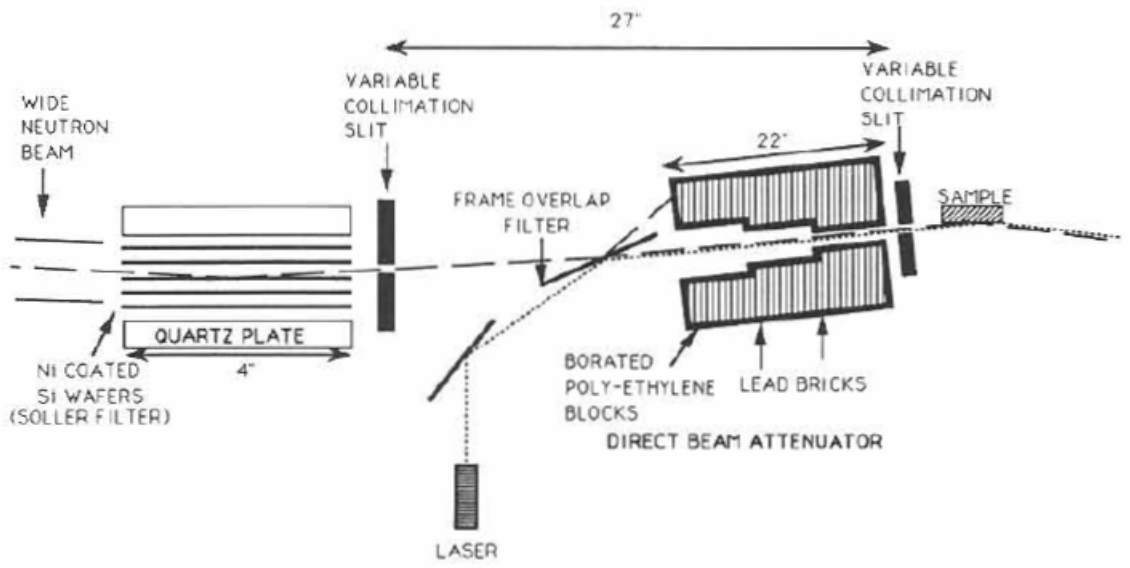

Figure 7: Detailed scheme of ^{58}Ni filters installed at *POSYII* (captured from the paper by Karim[20])

moderated by a solid methane moderator with an effective mean temperature of 30K. The neutron beam spectrum is redefined by two reflection ^{58}Ni filters and the detailed scheme of the filter assembly is shown in the Fig. 7[19]. The first filter consists of the 12 Si wafers and the second filter is a single Si wafer, coated with ^{58}Ni. Passing through the first filter set at an angle of 0.3°, all the neutrons with wavelength larger than 2.5Å are reflected toward the beam line. The second filter set at an angle of 1.8° reflects all the neutrons larger than 16Å and the remaining passes through the filter onto the sample stage. Thus, the range of neutron wavelength from 2.5 to 16Å is used to illuminate the sample. The redefined wavelength spectrum provides the time resolution, $\Delta t/t = 1\%$.

The intensities reflected at a set of discrete angles are collected by a one dimensional position sensitive detector as a function of the neutron wavevector k perpendicular to the surface. The wavevector is determined by the angle of the incident beam with the surface and the neutron wavelength. The angle(θ) of the incident beam has the range from 0 to 3° with the fixed angular resolution, $\Delta\theta/\theta = 5\%$. An assembly of ^3He gas filled linear detectors has 256 position channels with the uniform width. Each position channel is correspondently

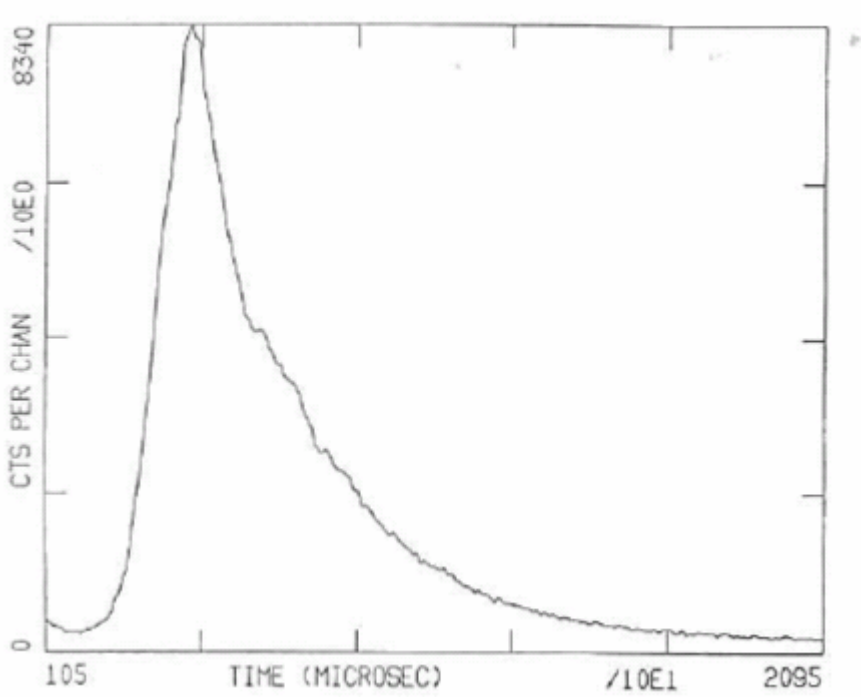

Figure 8: The time-dependent spectrum of the neutron beam of POSYII : the wavelength converted as $\lambda\left(\text{Å}\right) \simeq 5 \times 10^{-4} t\,(\mu\text{sec})$
(captured from the paper by Karim[20])

assigned into 256 time-of-flight channels. Fig. 8 shows the time-dependent spectrum of the neutron beam observed at the detector. The time-dependent spectrum of the neutron beam is converted to the wavelength as

$$\lambda\left(\text{Å}\right) = 4.0 \times 10^{-4} t\,(\mu\text{sec})\,/d\,(m) \simeq 5.0 \times 10^{-4} t\,(\mu\text{sec}) \tag{18}$$

where $t\,(\mu\text{sec})$ is the time measured from t_0 and $d\,(m)$ is the distance between the moderator and the detector($\sim 7.9m$)[19].

NR experiments were carried out with the sample changer and the discrete angles were set as 0.4, 0.9, 1.5 and 2.5°. These angles fully covered the reflection range from the critical edge to the first order diffraction peak and even the higher order peak. At every angle, the neutrons arriving at each position channel of the detector were counted until the preset number of pulses was collected. To obtain better statistics in counting the neutrons, the set of collecting pulses was repeated especially at a high angle.

Fig. 9, 10, and 11 show the neutron reflectivity results of the MLs obtained at POSY II, ANL and the data fit results using *reflfit*[6]. The actual BL spacing of each ML was estimated, based on the position(Q-value) of the 1st order diffraction peak.

0.3 Analysis and Discussion

0.3.1 Neutron scattering length densities from data-fit

In order to identify the structure from the scattering result, a data-fit process using a proper model structure is required due to the nature of scattering experiments. The scattering intensities are only recorded without any phase information that directly reveals the structure in the relation of Fourier transformation. Once a proper model structure is constructed, all the scattering parameters such as thickness, SLD, and roughness are determined according

[6]programmed by *P. A. Kienzle*, a scientist of National Institute of Standards and Technology(NIST)

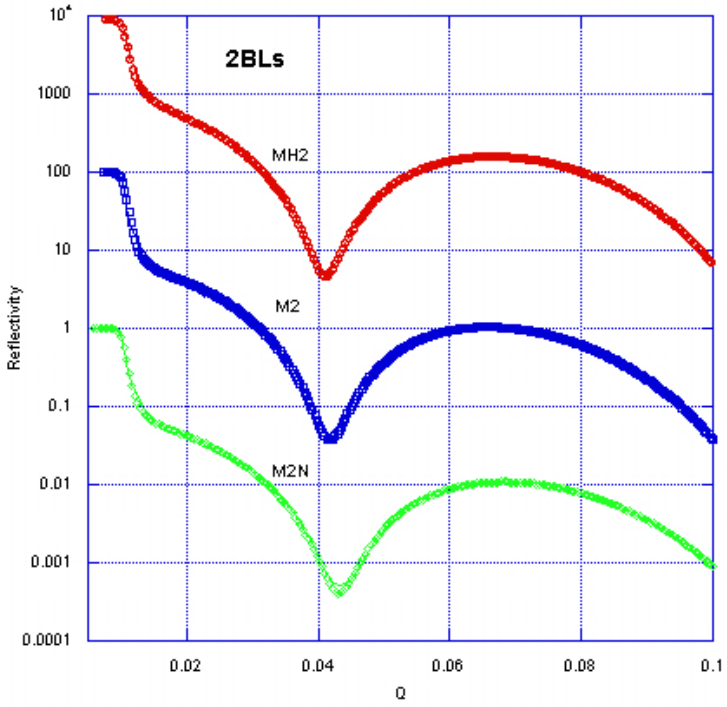

(a) 2 BLs

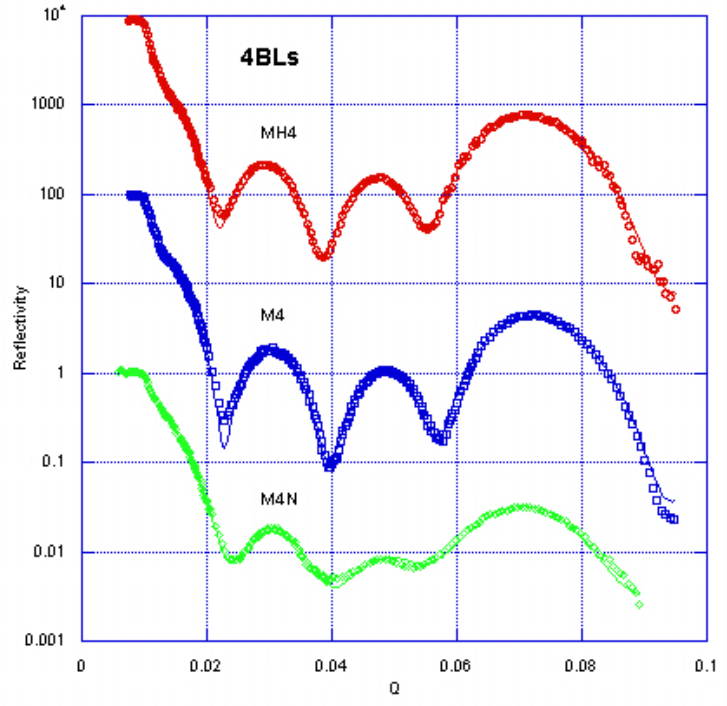

(b) 4 BLs

Figure 9: Neutron reflectivity data-fit of 2BL and 4BL

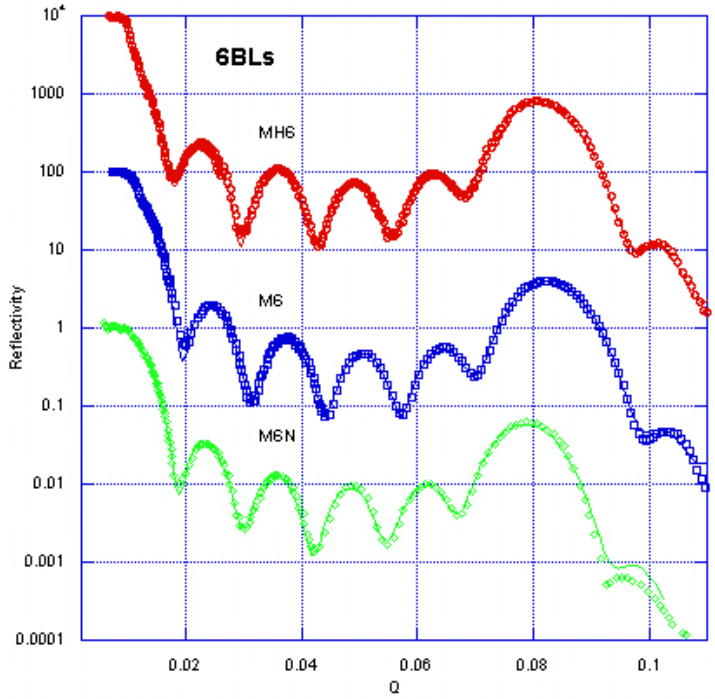

(a) 6 BLs

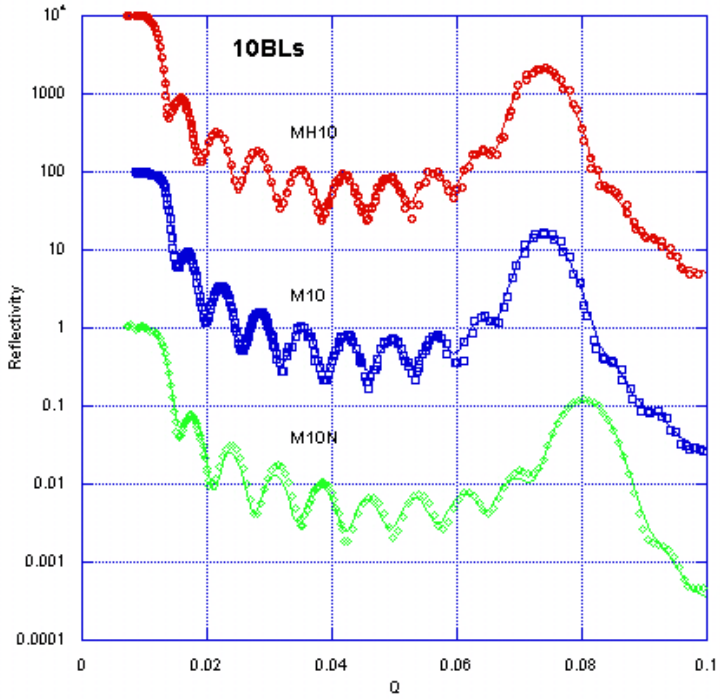

(b) 10 BLs

Figure 10: Neutron reflectivity data-fit of 6BL and 10BL

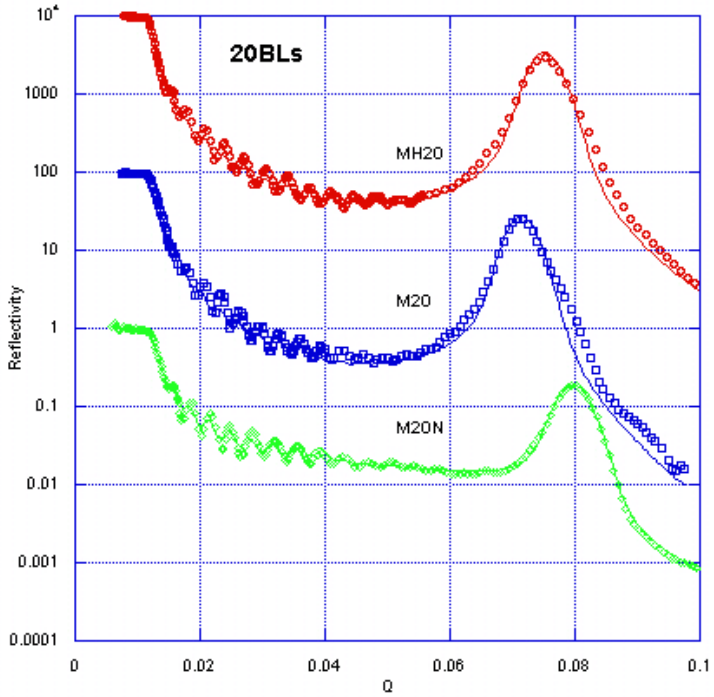

(a) 20 BLs

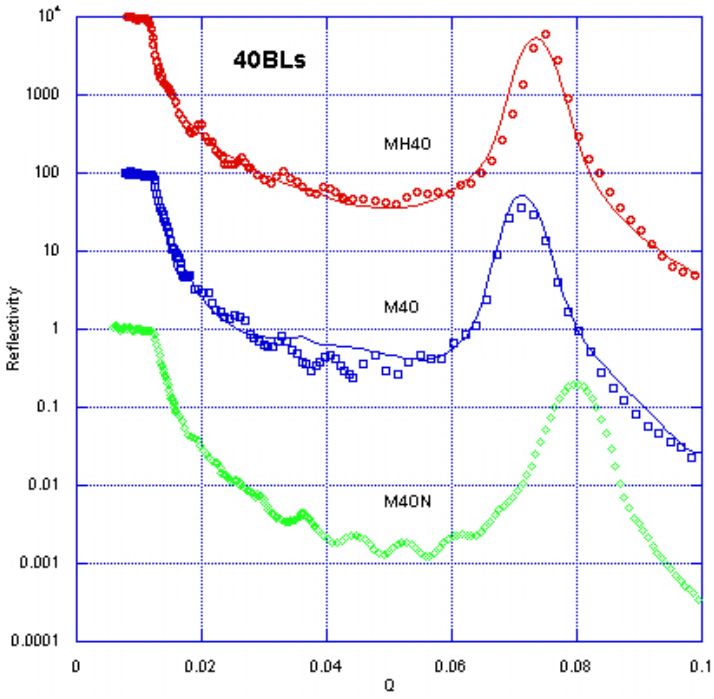

(b) 40 BLs

Figure 11: Neutron reflectivity data-fit of 20BL and 40BL

to the component materials. However, the data-fit result is not a unique solution for a scattering result because the complexity of the scattering parameters in the data-fit process can easily yield a number of reasonable solutions to the reflectivity. Even though the model structure obtained from the data-fit cannot confirm the real structure self-consistently, the average values of SLDs from all the data-fit results on the ML reflectivity measurements can lead to a tendency in the estimated SLDs. The average SLDs $\left[10^{-6}\text{Å}^{-2}\right]$ are 9.60 for Ni, -1.94 for Ti, -5.09 for TiH_2, and 2.08 for Si, which are overally corresponding to the calculated values above and the reference values in the Table 1. The data-fit results prove the hydrogen effect on the contrast enhancement between Ni and Ti layers can be explicitly estimated to be improved by $\sim 27.2\%$ coinciding well with the enhancement in the reference values between Ti and TiH_2.

0.3.2 Enhanced contrast between neutron scattering length densities

Comparison with the absolute reflectivities cannot be interpreted to the hydrogen effect on the reflection performance. Since the reflectivity is strongly dependent on the BL period and the SLD contrast, the remarkable differences in the BL spacing and the contrast among the sample with the same number of BLs produce in considerable variation of the reflectivity performance. Thus, the reflectivities of all the MLs should be normalized to the performance index that is independent from the structure factors. Accordingly, the neutron reflectivities measured at *POSYII* were normalized by the calculated reflectivity according to the BL spacing(d), the number of BLs(N), and the contrast($\Delta\rho b$) between pure Ti and Ni. The normalized reflectivities with the contrast between pure components explicitly explain how the addition of hydrogen atoms into Ti layers relatively improves the reflectivity performances under the conditions independent on the BL spacing.

As shown in Fig. 12, the obvious elevation in the reflectivity performance of the MH

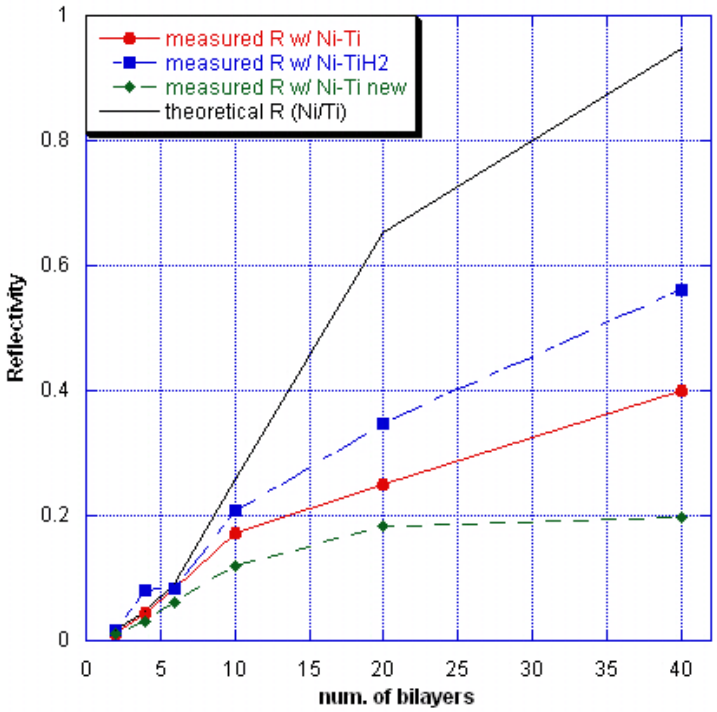

(a) Reflectivities measured from MLs

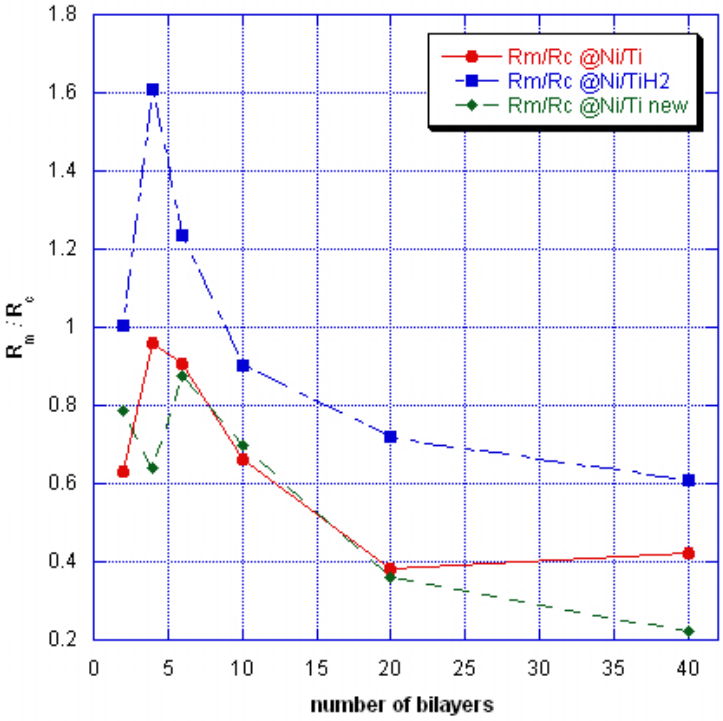

(b) $R_{measured}/R_{calculated}$ of MLs

Figure 12: Reflectivity analysis

set is observed and the average improvement in the normalized reflectivities in the MH set is $\sim$ 53.3% to the M set and $\sim$ 87.9% to the M new set. The contrast due to the addition of hydrogen atoms into Ti layers was enhanced by $\sim$ 27.2% and the enhanced contrast contributed for the enhanced reflectivity performance in the relation with the Eq. 17. Even though the reflectivity is sensitive to the change in the scattering parameters, only the enhanced contrast cannot improve the reflectivity performance as much as the obtained in the NR measurements. Since the interfacial roughness also plays a crucial role in the reflection, the improved reflectivities more than expected only with the contrast enhancement provides the possibility that the interfaces between the layers may be smoothened. Thus, the hydrogen effect on the interfacial roughness should be also considered.

0.3.3 Improved interfacial roughness

The Debye-Waller factor in the theoretical reflectivity was introduced by Saxena[9], in order to explain the measured reflectivity lower than the expected. An exponential term, the Debye-Waller factor, consists of the 1st order Bragg's diffraction peak position(Q) due to the bilayer spacing and the root-mean-square roughness (σ_{rms}). Therefore, the theoretic reflectivity for the 1st order Bragg's diffraction peak is expressed as

$$R = \exp\left(-Q^2\sigma_{rms}^2\right) R_0 = \exp\left(-Q^2\sigma_{rms}^2\right) \tanh^2\left(\frac{2Nd^2\Delta\rho b}{\pi}\right) \tag{19}$$

Using the relation of $Q = \frac{2\pi}{d}$, the Q values of the peak positions were obtained from the NR results(Table 2) and the σ_{rms} values were calculated in three different ways:

1. Debye-Waller factor$[\exp\left(-Q^2\sigma_{rms}^2\right)]$ is constant ; the contrast and the Debye-Waller factor were from the data-fit on the reflectivity versus Nd^2 as fitting parameters and then each σ_{rms} for individual sample was calculated.

2. The hydrogen concentration was considered for calculating the contrast $\Delta\rho b$; the

contrast was calculated according to the hydrogen concentration and then used to calculate R_0. The ratio of R/R_0 gives the Debye-Waller factor and σ_{rms} was obtained from this result .

3. The theoretical contrasts for Ni/Ti and Ni/TiH_2were used ; the theoretical contrasts were employed to calculate R_0.

As shown in Fig. 13, the Debye-Waller factor analyses explain how the hydrogen effect on the interfaces dramatically improves blurriness especially over 20 BLs. From this analysis, hydrogen smoothes the interfacial roughness caused by the preferential directions of growth of Ni and Ti or the interdiffusion between Ni and Ti layers. In order to obtain high reflectivity close to 1, a enormous number of BLs are required in the fabrication of a high performance ML structure. The addition of hydrogen can benefit in not only smoothening the interfaces by suppressing the irregularity of the interfaces but also reducing the required number of BLs by enhancing the contrast.

0.3.4 Interfacial roughness analysis

Using *slow* AES technique, the interfaces can be studied from the point of microscopical view. Based on AES analysis, a new parameter was introduced by *Tadayyon* to evaluate the interfacial interdiffusion and roughness[20]. The parameter f is defined by

$$f = \Delta \mathrm{I} \times \frac{t}{S} \tag{20}$$

As denoted in the Fig. 14, ΔI is the net intensity at the centroid of each peak and t is the time between the minima of the peak. S is the area integrated under the peak. The concentration modulation amplitude was used to explicitly figure out the interlayer diffusion. It was reported that the f-parameters respond to the interdiffusion of the species and that the Arrhenius-type temperature dependence of the diffusion coefficients D was evaluated[20]

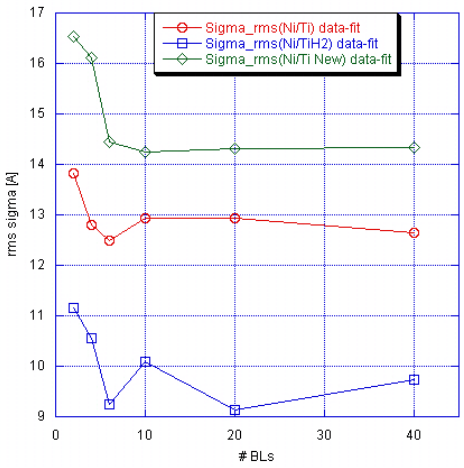

(a) $\sigma_r ms$ in Debye-Waller from data-fit

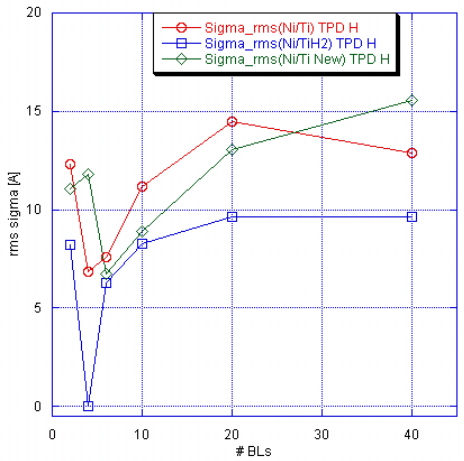

(b) $\sigma_r ms$ in Debye-Waller with the hydrogen concentration

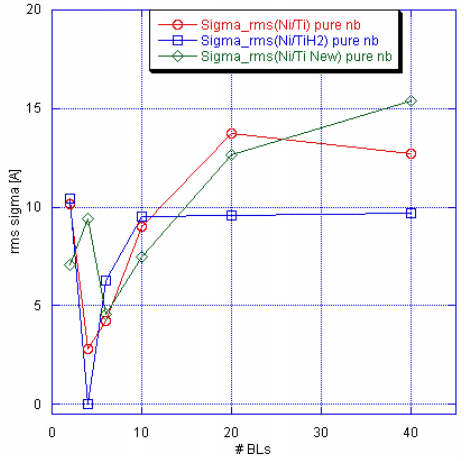

(c) $\sigma_r ms$ in Debye-Waller with the pure contrasts

Figure 13: Debye-Waller factor analysis

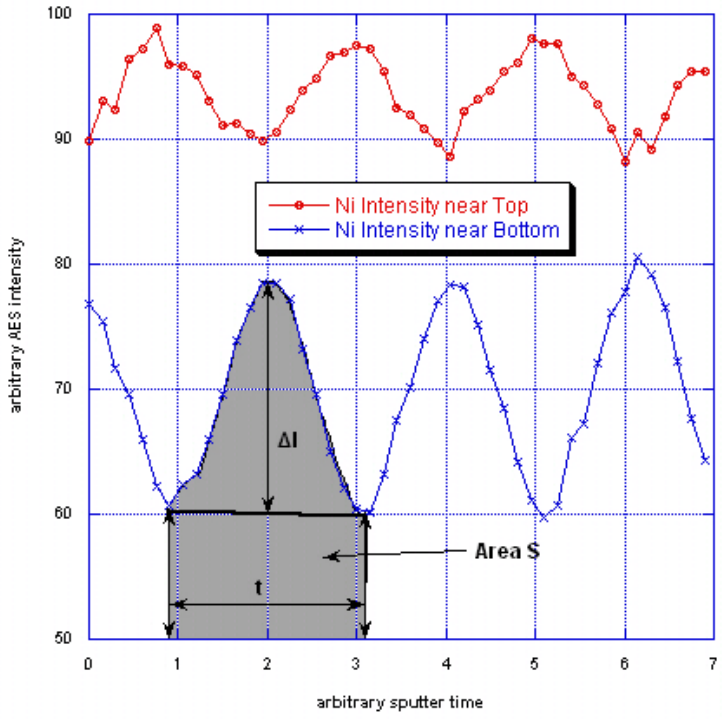

(a) Interfaces of Ni in a ML sample

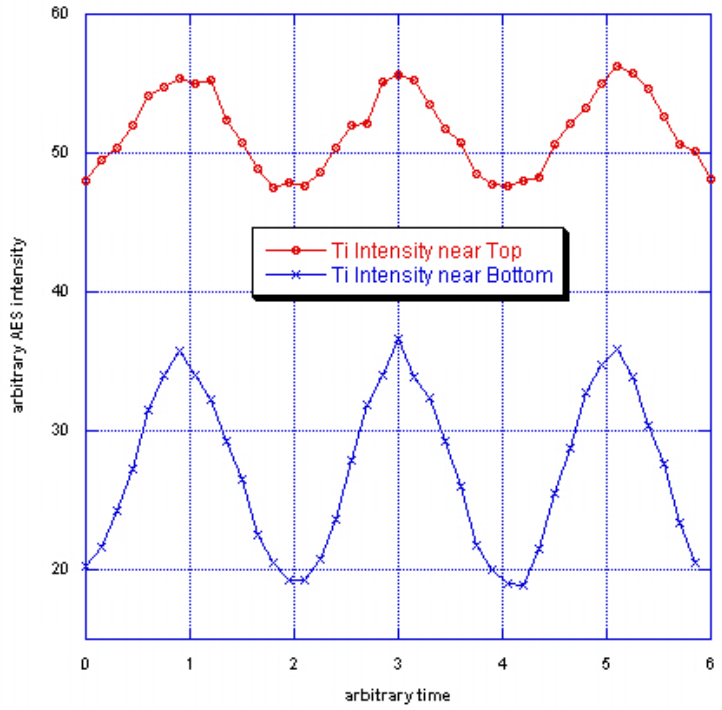

(b) Interfaces of Ti in a ML sample

Figure 14: Interface comparison from the bottom layer to the top Layer

as

$$D = D_0 \exp\left(-Q/RT\right) \tag{21}$$

where $D_0 = 3 \times 10^{-11}\ m^2/s$ and $Q = 120\ kJ/mol$ for pure-Ni AES and $D_0 = 7 \times 10^{-10}\ m^2/s$ and $Q = 130\ kJ/mol$ for pure-Ti AES.

The concentration peak with the blurry interface has the bigger area and the lower amplitude. Thus, from the definition, the f-parameters of those peaks are lower than the others. The lower f-parameter for a peak may imply that the interlayer diffusion from the peak is more active than the diffusion from the other peaks with the higher f-parameter[20].

From *Kumar*, improving the reflectivity was accomplished by choosing reactive sputtering of Ni layers in a mixture of Ar and air for suppressing the interdiffusion between BLs[21, 22]. On the other hand, according to *Elsenhans*, the interdiffusion could be restrained by addition of C into Ni and H into Ti and hydrogenation turned out to be more effective[23, 24]. The hydrogen effect on the interfaces as a diffusion barrier can be proven by comparing the slopes of the f-parameters. However, the f-parameters of each sample cannot be interpreted into the standardized direct effect of H addition. Thus, the f-parameters in different samples should be normalized with the standard f-parameter, f_o. The parameter f_o was defined differently as to the definition of f_o by *Tadayyon;* the peak with the highest f was picked among the first three peaks nearest the substrate and then all f-parameters were reciprocally normalized with f_o as f_o/f. This ratio shows the relative blurriness of each component layer(Ni and Ti or TiH_x) compared to the sharpest peak that is thought as the primary layer profile. Shown in Fig. 15, the interfaces of the MLs with lower H concentration exponentially get blurry, whereas relatively higher H concentration maintains the blurriness by suppressing the interdiffusion.

Ideally, the diffusion barriers restrain the interdiffusion between alternative layers and the additive atoms at the interstitial sites get the interfaces smoother. Therefore, the H addition into Ti not only improves the SLD contrast by introducing more negative SLD into

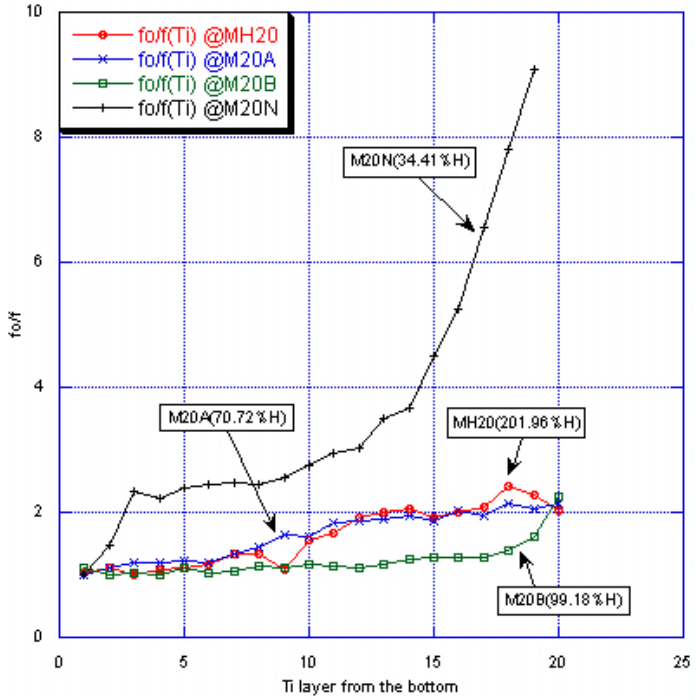

(a) $\frac{f_o}{f}$ of Ti layers in 20BLs

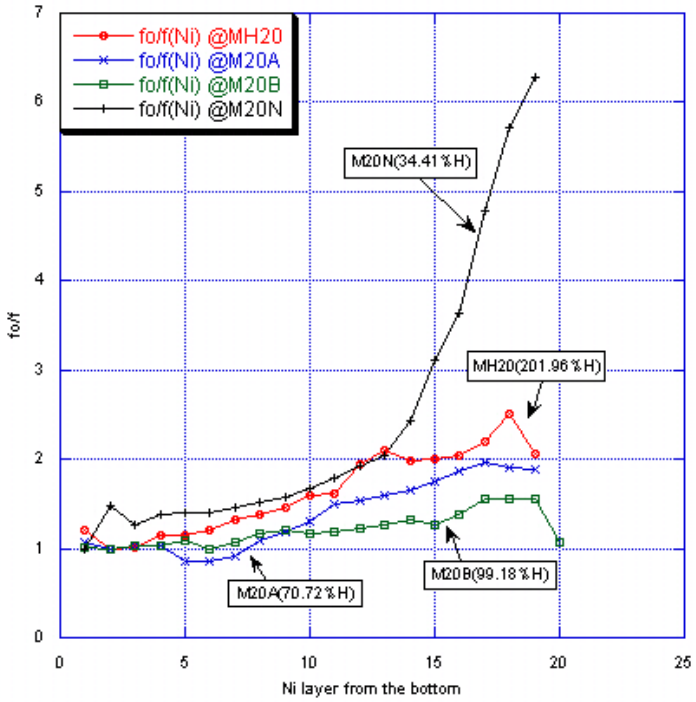

(b) $\frac{f_o}{f}$ of Ni layers in 20BLs

Figure 15: f_o/f parameters of 20 BLs

Ti but also reduces the interfacial roughness by smoothening the interfaces and suppressing the interdiffusion.

0.4 Conclusion

The effect of hydrogen addition into Ti layers was proved by the significant elevation in neutron reflectivity responses from all samples. Comparision between the normalized reflectivities of 'with-H' and 'without-H' ML sets resulted in the improvement of the first order diffraction peak intensities by $\sim 53.3\%$ from Ni/Ti set and $\sim 87.9\%$ from new Ni/Ti set. In the specular mirror reflection, the SLD contrast and the roughness of ML films heavily contribute to the reflectivity. The incorporation of hydrogen with Ti turned out to enhance the SLD contrast, $\Delta\rho b$, between Ni and Ti by $\sim 27.2\%$. The improved reflecivity responses of the MLs with hydrogen were also attributed to sharpening the interfaces. Both of Ni/TiH_2 and Ni/Ti sets, however, showed less intensity at the first order diffraction peak intensities than the expected. The lower performances of the MLs may be caused from the thickness variation during the sample preparation.

In conclusion, the addition of hydrogen into Ti layers significantly improved the reflectivity of the $Ni-Ti$ MLs by enhancing the SLD contrast between Ni and Ti and smoothening the interfacial roughness. The incorporation of hydrogen changed the topograph of the surface toward being amorphous and restrained the interdiffusion as a diffusion barrier. Moreover, the improved reflectivity can dramatically reduce the total number of the BLs required to produce the first order diffraction peak intensity close to 1. From the incremental tendency in the roughness, the less number of the BLs greatly benefits from minimizing the roughness and simultaneously maximizing the reflectivity. Thus adding hydrogen into Ti should be considered seriously as a fine solution for fabricating a neutron optics device with the ML structure such as a monochromator, a neutron guide and a suppermirror.

Acknowledgments

This project was supported by the U. S. Department of Energy(DOE) Innovations in Nuclaer Education and Infrastructure(INIE) program under the contract number Pu-2406-UI-4423. The experiments were supported by the U. S. Department of Energy, Division of Material Sciences under Award number DEFG02-91ER45439, through the Frederick Seitz Materials Research Laboratory(FS-MRL) at the University of Illinois at Urbana-Champaign(UIUC), and backed up by the Intense Pulsed Neutron Source(IPNS), Argonne National Laboratory, funded by the U. S. Department of Energy, Basic Energy Sciences under Contract number W-31-109-ENG-38 to the University of Chicago. This research would not have been possible without the supports of many people. The help and the assistance of Mauro Sardela, Nancy Finnegan, Scott McLaren, Tony Banks, and Vania Petrova, FS-MRL, UIUC are gratefully acknowledged. Finally, the assistance of R. Goyette(ORNL) and S. Park(KBSI) is also appreciated.

Bibliography

[1] I. S. Anderson, Neutron Data Booklet:3.2-1 Neutron Optics, Neutrons For Science, 2002.

[2] J. B. Hayter, H. Mook, Discrete Thin-Film Multilayer Design for X-ray and Neutron Supermirrors, J. Appl. Cryst. 22 (1989) 35–41.

[3] J. Lekner, Reflection Theory and the Analysis of Neutron Reflection Data, Physica B 173 (1991) 99–111.

[4] V. F. Sears, Neutron Optics, Oxford University Press, Inc., 1989.

[5] B. P. Schoenborn, D. L. D. Caspar, O. F. Kammerer, A Novel Neutron Monochromator, J. Appl. Cryst. 7 (1974) 511–512.

[6] V. F. Sears, Theory of Multilayer Neutron Monochromators, Acta. Cryst. A 39 (1983) 601–608.

[7] V. F. Sears, Dynamical Diffraction in Periodic Multilayers, Acta. Cryst. A53 (1997) 649–662.

[8] J. Padiyath, J. Stahn, M. Horisberger, Multilayers with tailored blurred interfaces, Appl. Phys. Lett. 89 (2006) 113123.

[9] A. M. Saxena, B. P. Schoenborn, Multilayer Neutron Monochromators, Acta. Cryst. A33 (1977) 805–813.

[10] F. Mezei, Novel polirized neutron devices:supermirror and spin component amplifier, Communications on Physics 1, n3 (1976) 81–5.

[11] T. Ebisawa, N. Achiwa, S. Yamada, T. Akiyoshi, S. Okamoto, Neutron Reflectivities of Ni-Mn and Ni-Ti Multilayers for Monochromators and Supermirrors, J. Nuc. Sci. & Tech. 16 (1979) 647–659.

[12] A. M. Saxena, High-Reflectivity Multilayer Monochromators for Neutrons, J. Appl. Cryst. 19 (1986) 123–130.

[13] M. Hino, H. Sunohara, Y. Yoshimura, R. Maruyama, S. Tasaki, H. Yoshino, Y. Kawabata, Recent Development of Multilayer Neutron Mirror at KURRI, Nuc. Inst. Methods in Phys. Research A 529 (2004) 54–58.

[14] H. L. Y. Jnr, Thermocrystallography of Higher Hydrides of Titanium and Zirconium, Acta. Cryst. 11 (1958) 46–51.

[15] R. Sailer, G. M. N. D. S. Univ.), Code num. 44-1294, JCPDS-International Centre for Diffraction Data (1993).

[16] P. R. Mallory, C. A. Suggs, Code num. 03-0859, JCPDS-International Centre for Diffraction Data (1957).

[17] K. Oura, V. G. Lifshits, A. A. Saranin, A. V. Zotov, M. Katayama, Surface Science : An Introduction, Springer, 2003.

[18] N. Finnegan, Physical Electronics PHI 660 Scanning Auger Microprobe (http://cmm.mrl.uiuc.edu/instruments/660.htm), the web site, http://cmm.mrl.uiuc.edu/instruments/660.htm.

[19] A. Karim, B. H. Arendt, R. Goyette, Y. Y. Huang, R. Kleb, G. P. Felcher, An Automated Neutron Reflectometer (POSY II) at the Intense Pulsed Neutron Source, Physica B 173 (1991) 17–24.

[20] S. M. Tadayyon, O. Yoshinari, K. Tanaka, Auger Electron Spectroscopy and X-ray Diffraction Study of Interdiffusion and Solid State Amorphization of Ni/Ti Multilayers, Jpn. J. Appl. Phys. 31 (1992) 2226–2232.

[21] M. S. Kumar, P. Böni, S. Tixier, On the Reflectivity of Reactively Sputtered Ni/Ti Multilayers, Physica B 241-243 (1998) 95–97.

[22] M. S. Kumar, P. Böni, S. Tixier, D. Clemens, Stress Minimisation in Sputtered Ni/Ti Supermirrors, Physica B 241-243 (1998) 95–97.

[23] O. Elsenhans, P. Böni, H. P. Friedli, H. Grimmer, P. Buffat, K. Leifer, I. Anderson, Thin Films for Neutron Optics, SPIE Neutron Optical Devices and Applications 1738 (1992) 130–140.

[24] O. Elsenhans, P. Böni, H. P. Friedli, H. Grimmer, P. Buffat, K. Leifer, J. Söchtig, I. S. Anderson, Development of Ni/Ti multilayer supermirrors for neutron optics, Thin Solid Films 246 (1994) 110–119.